Pergamon

Journal of Structural Geology, Vol. 18, No. 4, pp. 395 to 411, 1996

0191-8141/96 $15.00+0.00

0191-8141(95)00095-X

Deformation partitioning and foliation reactivation during transpressional orogenesis, an example from the Central Longmen Shan, China

BRENTON A. WORLEY and CHRISTOPHER J. L. WILSON

School of Earth Sciences, The University of Melbourne, Parkville, Victoria 3052, Australia

(*Received* 21 *November* 1994; *accepted in revised form* 26 *July* 1995)

Abstract—Progressive localization of strain within the Songpan–Garzê Fold Belt, at the eastern margin of the Tibetan Plateau, has resulted in the formation of the Wenchuan–Maowen Shear Zone and preservation of excellent overprinting relationships between three major phases of ductile and semi-ductile deformation. These relationships show that deformation in the eastern Songpan–Garzê Fold Belt evolved from crustal thickening during SW-directed compression (D_1) to localized sinistral transcurrent shear (D_2) and finally to increasingly localized high temperature (D_{3p}) and retrograde (D_{3r}) reverse shear in response to SE-directed compression. Both D_2 and D_3 deformations were co-planar and reactivation of the S_2 foliation led to the formation of a composite S_{2-3} fabric. However, inclusion trails in garnet porphyroblasts preserve evidence of a transition between these strike-slip and reverse shear end members, indicating that D_2 and D_3 were part of an episode of progressive transpressional shear. Metamorphic grade increases from chlorite to kyanite zone within the Wenchuan–Maowen Shear Zone, reaching syn-D_{3p} peak conditions of ~600°C and 10 kbar. The D_{3p} and D_{3r} reverse shears were responsible for tectonic exhumation of the shear zone and resulted in the formation of retrograde D_{3r} high strain zones along the margins of the Xuelongbao Granite and adjacent to the Wenchuan–Maowen Fault.

INTRODUCTION

Localization of deformation in ductile shear zones is a common crustal feature related to either syntectonic processes and/or the superposition of later deformation episodes into a zone of pre-existing deformation. Along the margins of the Tibetan Plateau, i.e. in the Himalayan Mountains and Longmen Shan (shan = mountains), these localized zones of deformation may be several kilometers wide (Butler & Prior 1988, Burg & Chen 1984, Dirks *et al.* 1994). In attempting to deduce a plausible structural history for these multiply deformed zones of localized strain, it is necessary to determine the nature and orientation of early formed fabrics which have since been destroyed by the progressive deformation. A useful technique for gathering such information is to study the microstructures developed in strain shadows adjacent to relatively rigid bodies such as porphyroblasts and quartz boudins and, more specifically, the relationship between internal foliations preserved in porphyroblasts and the external foliation in the surrounding matrix. Numerous recent studies using such methods have highlighted the progressive nature of deformation in orogenic belts and the importance of processes such as the reactivation of early fabrics and the formation of composite foliations (Meneilly 1982, Bell & Rubenach 1983, Tobisch & Paterson 1988, Bergh & Karlstrom 1992, Davis 1993, 1994, Davis & Forde 1994). In this paper, we present field data from the central Longmen Shan of China (Fig. 1), where progressive localization of deformation, with time, has resulted in the excellent preservation of overprinting relations between several generations of fabrics. This localization has enabled us to investigate the roles of deformation partitioning, fabric reactivation and composite foliation development in the formation of the observed macro-, meso- and microscopic structures and illustrate the importance of recognizing such processes when attempting to reconstruct the structural history of orogenic belts.

GEOLOGICAL FRAMEWORK

The Songpan–Garzê Fold Belt occupies a large portion of the eastern Tibetan Plateau and is separated from the major hydrocarbon-producing Sichuan Basin to the east by the Longmen Shan Thrust–Nappe Belt (Fig. 1; Chen *et al.* 1995). The fold belt and Sichuan Basin are both underlain by crystalline Proterozoic basement (Chen *et al.* 1995) but have distinctly different Phanerozoic sedimentary and structural histories. Composed of a Palaeozoic–Mesozoic sequence of predominantly deep water shale, fine sandstone and extensive turbidites (Fig. 2), the Songpan–Garzê Fold Belt was deformed and metamorphosed during the Late Triassic (Norian–Rhaetian) Indosinian Orogeny (Hu 1987, Hu & You 1991, Dirks *et al.* 1994, Chen *et al.* 1995). Extensive S- and I-type granite magmatism (Liu *et al.* 1984, Yuan *et al.* 1991) accompanied and outlasted the orogeny. Granite plutons cross-cut stratigraphy and early deformational fabrics, and generally have contact metamorphic aureoles up to 2–4 km in width (Dirks *et al.* 1994).

The Sichuan Basin remained stable throughout most of the Indosinian Orogeny and subsequently the Sinian–Upper Triassic (T_3^2) stratigraphy is dominated by shallow marine, platform carbonates. However, in the final stages of the orogeny, the Longmen Shan Thrust–Nappe

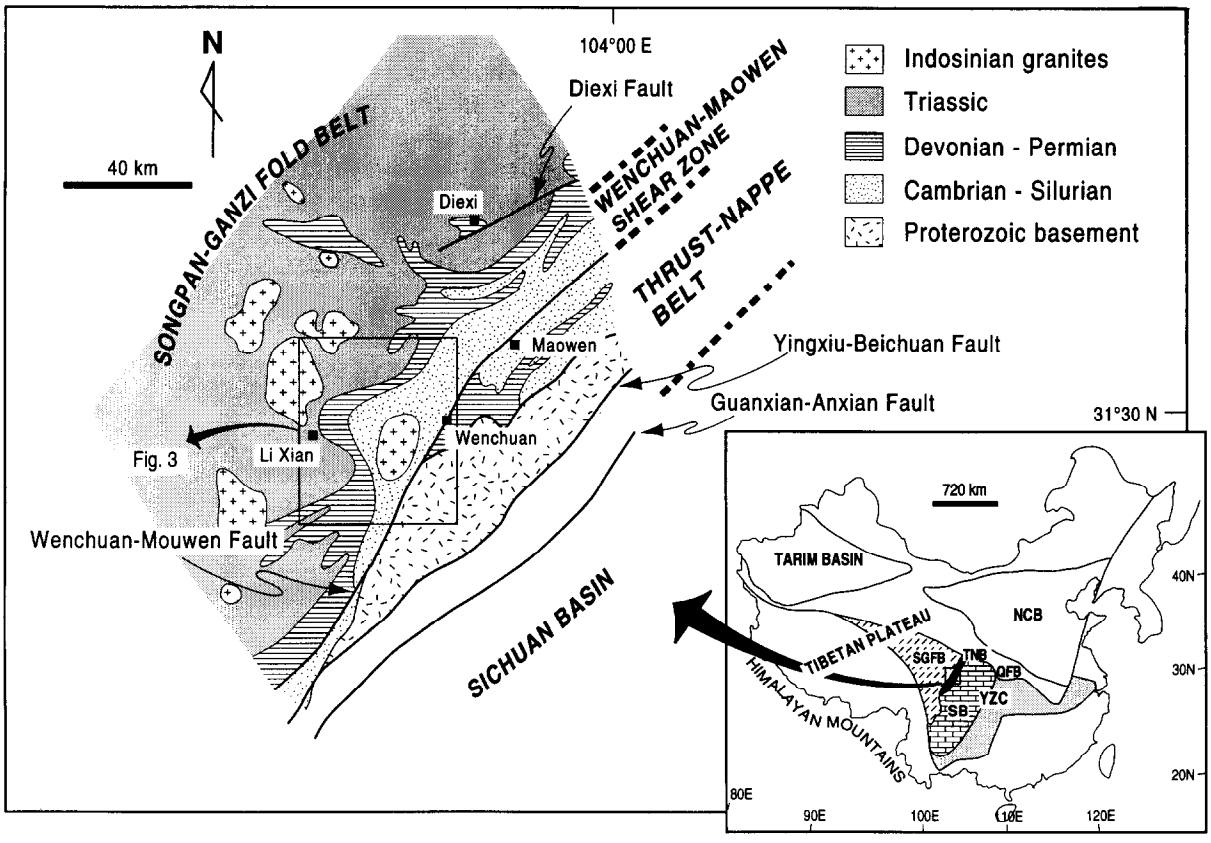

Fig. 1. Simplified geological map of the central Longmen Shan, illustrating the relationship between the Songpan–Garzê Fold Belt (SGFB), Longmen Shan Thrust–Nappe Belt (TNB) and Sichuan Basin (SB). These tectonic units are bounded by the symbols: NCB = North China Block, YZC = Yangtze Craton, QFB = Qiling Fold Belt.

Belt was initiated and propagated eastward onto the western Sichuan Basin. This resulted in the formation of the Western Sichuan Foreland Basin with sporadic terrestrial deposition from Late Triassic (T_{3x}) to Quaternary (Chen *et al.* 1994).

Three principal episodes of ductile to semi-ductile Indosinian deformation have been recognized in the eastern Songpan–Garzê Fold Belt (Wilson *et al.* 1994, Worley *et al.* 1995, Chen *et al.* 1995). The accumulation of differential strain along the eastern margin of the fold belt resulted in partitioning of deformation into the 20–25 km wide Wenchuan–Maowen Shear Zone (Fig. 3; Dirks *et al.* 1994, Worley *et al.* 1995). NE-trending structures, developed in the shear zone during D_2 as the result of sinistral shear, are partially overprinted by coplanar D_3 structures formed during uplift of the Songpan–Garzê Fold Belt in response to SE-directed compression.

The Songpan–Garzê Fold Belt has, as a whole, undergone lower greenschist facies (chlorite zone) metamorphism, while localized high strain zones along the margins of the belt, i.e. the Wenchuan–Maowen Shear Zone and Diexi Fault (Fig. 1; Dirks *et al.* 1994), experienced upper greenschist–amphibolite facies conditions. Peak metamorphic conditions reached kyanite grade within the Shapai region of the Wenchuan–Maowen Shear Zone, adjacent to the Xuelongbao Granite (Fig. 3). The granite cross-cuts Palaeozoic sediments and deflects tectonic fabrics associated with the development of the shear zone (Fig. 3) but, unlike the other granites in the fold belt, there is no contact metamorphic aureole preserved.

DEFORMATION HISTORY OF THE WENCHUAN–MAOWEN SHEAR ZONE

Macro- and mesoscopic structures within the Wenchuan–Maowen Shear Zone and other regions of the eastern Songpan–Garzê Fold Belt can be described in terms of three main ductile to semi-ductile deformational episodes (D_1, D_2 and D_3). We appreciate the timing problems outlined by Tobisch & Paterson (1988) and do not infer that deformation occurred as three temporally discrete events. Rather, we use this nomenclature to relate the different structures to major changes in deformation style or orientation, which in a particular area or outcrop (but not necessarily over the orogen) maintain consistent overprinting relations. The preservation of the overprinting relationships is in part due to progressive localization of deformation into the Wenchuan–Maowen Shear Zone.

D_1

Upright–inclined F_1 folds (Fig. 4a) are developed throughout the Songpan–Garzê Fold Belt. Rheological contrasts have resulted in a large range of lithologically dependent fold styles. The fold shapes range from open

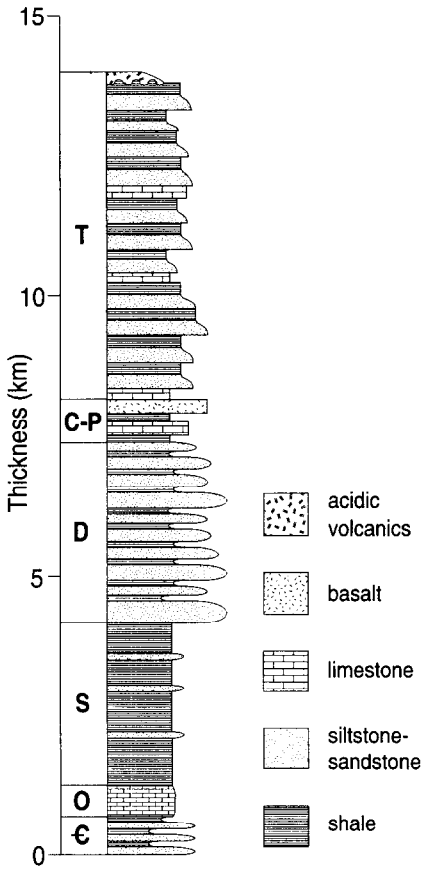

Fig. 2. Schematic log illustrating the Palaeozoic–Mesozoic stratigraphy of the Songpan–Garzê Fold Belt. The Palaeozoic sequence is dominated by greywacke and shale with the Triassic composed of turbiditic sediments.

in thick psammitic units to isoclinal in carbonate, shale, and turbiditic lithologies. In regions of low post-D_1 strain (i.e. the central portions of the fold belt), F_1 folds have shallow plunging axes and a pervasive NW–SE-striking, axial planar slaty cleavage (S_1), defined by an alignment of white mica, chlorite and elongate quartz; S_1 dips 60–90° to either the southwest or northeast (Fig. 3). As the Wenchuan–Maowen Shear Zone is approached and the fold belt is increasingly affected by D_2 strain, the D_1 structures have been progressively rotated into a northeast–southwest orientation (arcuate zone of Chen *et al.* 1995), and transposed into the S_2 fabric. Therefore, D_1 structures are not preserved in the high D_2 strain regions of the fold belt.

Limb thrusts and duplex structures are commonly associated with isoclinal F_1 folds. These structures, in conjunction with a consistent down-dip mineral elongation lineation, defined by elongate oxidation spots and quartz pressure shadows around pyrite porphyroblasts, indicate a general top-to-the-northeast sense of shear. Thrusting and folding during D_1 have resulted in greater than 50% shortening and hence thickening of the fold belt (Wilson *et al.* 1994).

D_2

Structures attributed to the D_2 event are spatially and temporally associated with the development of the Wenchuan–Maowen Shear Zone. Throughout the central portions of the Songpan–Garzê Fold Belt, D_2 structures are rarely developed, occurring only locally as regions of intense crenulation cleavage development and local refolding, adjacent to granite intrusions and in smaller high strain zones along the margin of the fold belt such as the Diexi Fault (Fig. 1).

The northwestern margin of the Wenchuan–Maowen Shear Zone is gradational, with D_2 strain increasing toward the southeast. The D_2 deformation is first evidenced by a sub-vertical, E–W-striking (Fig. 3) spaced crenulation cleavage (S_2) which is associated with steeply plunging, open F_2 folds (Figs. 4b & c). From northwest to southeast across the Wenchuan–Maowen Shear Zone, S_2 evolves from a spaced crenulation cleavage (cleavage seams $<100\,\mu$m in width) into a domainal crenulation cleavage (with mica-rich cleavage domains up to 10 mm in width) and finally into a pervasive slaty cleavage or schistosity, depending on metamorphic grade (Figs. 4c–e). Coincident with the evolution of the S_2 cleavage, F_2 folds are progressively tightened and assume a consistent sinistral asymmetry (Figs. 4d and 6). This evolution of the S_2 fabric is an excellent mesoscopic example of a complete cycle of schistosity development via a crenulation cleavage as proposed by Bell & Rubenach (1983) and can be attributed to increasing D_2 strain across the shear zone. At the microscopic scale, partitioning of deformation is more complex and in many thin sections four or more stages of Bell and Rubenach's cycle can be recognized in areas of less than 100 mm^2. At low strain, and low metamorphic grade (chlorite zone), deformation is strongest at the contacts between mica-rich and quartz-rich schist (Fig. 4b). Initial localization of the deformation is thus most likely the result of partitioning of strain from the more competent quartz-rich layers into the immediately adjacent mica-rich layers. Deformation has then been progressively localized along the limbs of asymmetric folds resulting in formation of thick cleavage seams (cl in Fig. 4b) and the preservation of stages 1 (no deformation) to 4 (differentiated crenulation cleavage with crystallization of new mica) of Bell and Rubenach's cycle. Thinning and truncation of quartz-rich layers by the cleavage seams indicates that quartz removal by pressure solution was an important deformation mechanism during crenulation cleavage formation under these conditions.

At higher metamorphic grades (garnet zone) and higher strain, partitioning of the deformation has once again resulted in the preservation of a range of S_2 fabrics (Figs. 4f and 6). An important factor controlling the extent of S_2 development is the thickness of mica-rich layers. In very fine mica-rich layers (2 in Fig. 4f), S_1 has been crenulated, and while S_1 micas exhibit kinking there is no evidence of new mica crystallization parallel to the axial surface of the microfolds (stages 2–3). In slightly thicker mica-rich layers (4 in Fig. 4f), the cleavage has reached stage 4 with crystallization of undeformed D_2 muscovite parallel to S_2. Crenulated S_1 muscovite is kinked and quartz commonly exhibits undulose extinction and sub-grain formation indicating

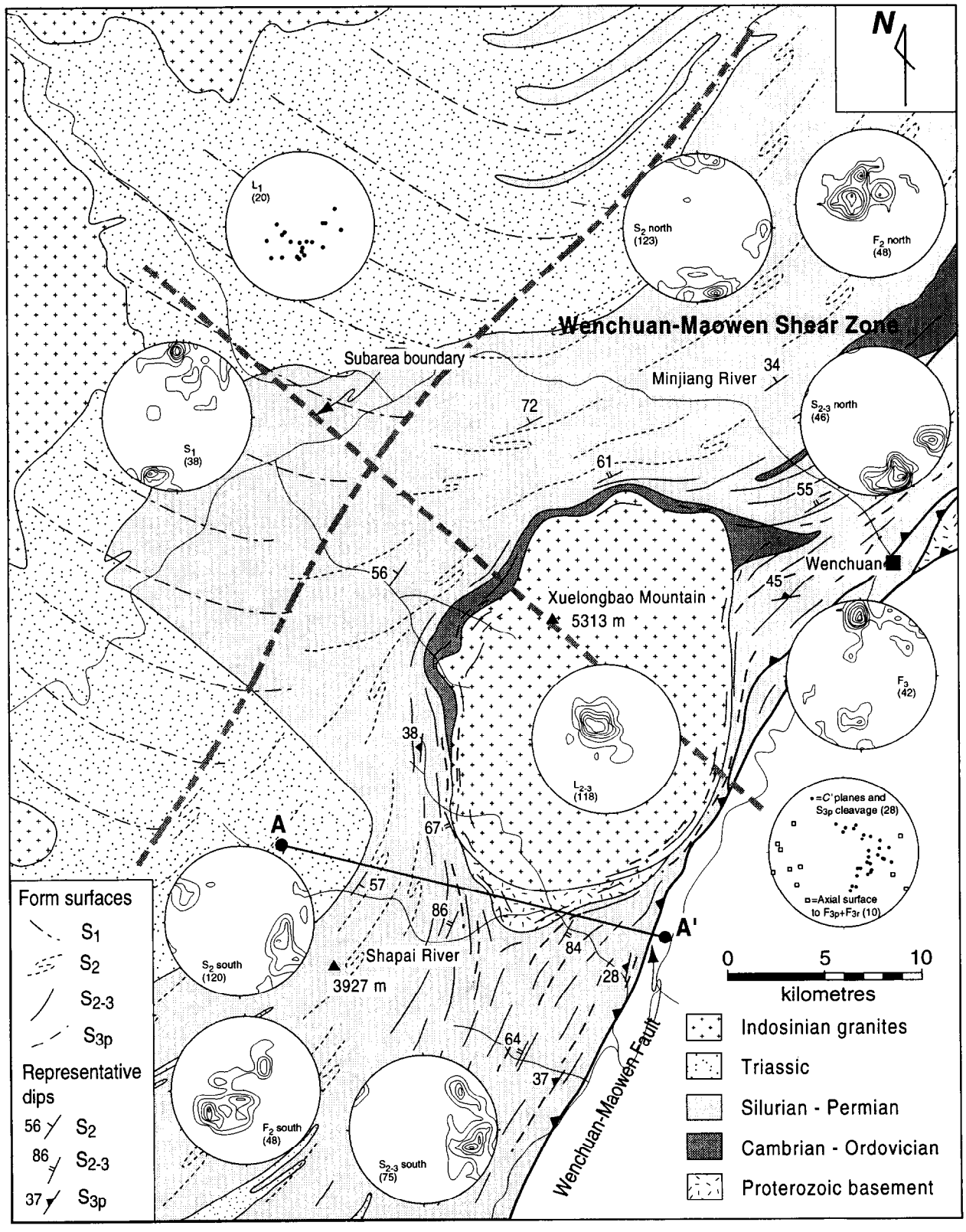

Fig. 3. Composite structural and geological map of the Xuelongbao region. All stereonets are lower hemisphere equal area projections, contour intervals are 2.0% per 1% area. Location of this area is indicated on Fig. 1 and cross-section A–A′ is shown in Fig. 9.

the importance of crystal plastic deformation mechanisms such as dislocation creep. Partitioning of strain around a garnet porphyroblast has resulted in the crenulation cleavage evolving to stage 5 (5 in Fig. 4f) and stage 6 (6 in Fig. 4f). Therefore, within a distance of <5 mm, the S_2 cleavage varies from open crenulations with no S_2 muscovite crystallization to a penetrative schistosity. At a slightly coarser scale (i.e. Fig. 6), a similar range in crenulation cleavage development is exhibited, with cleavage intensity increasing toward a long limb of an

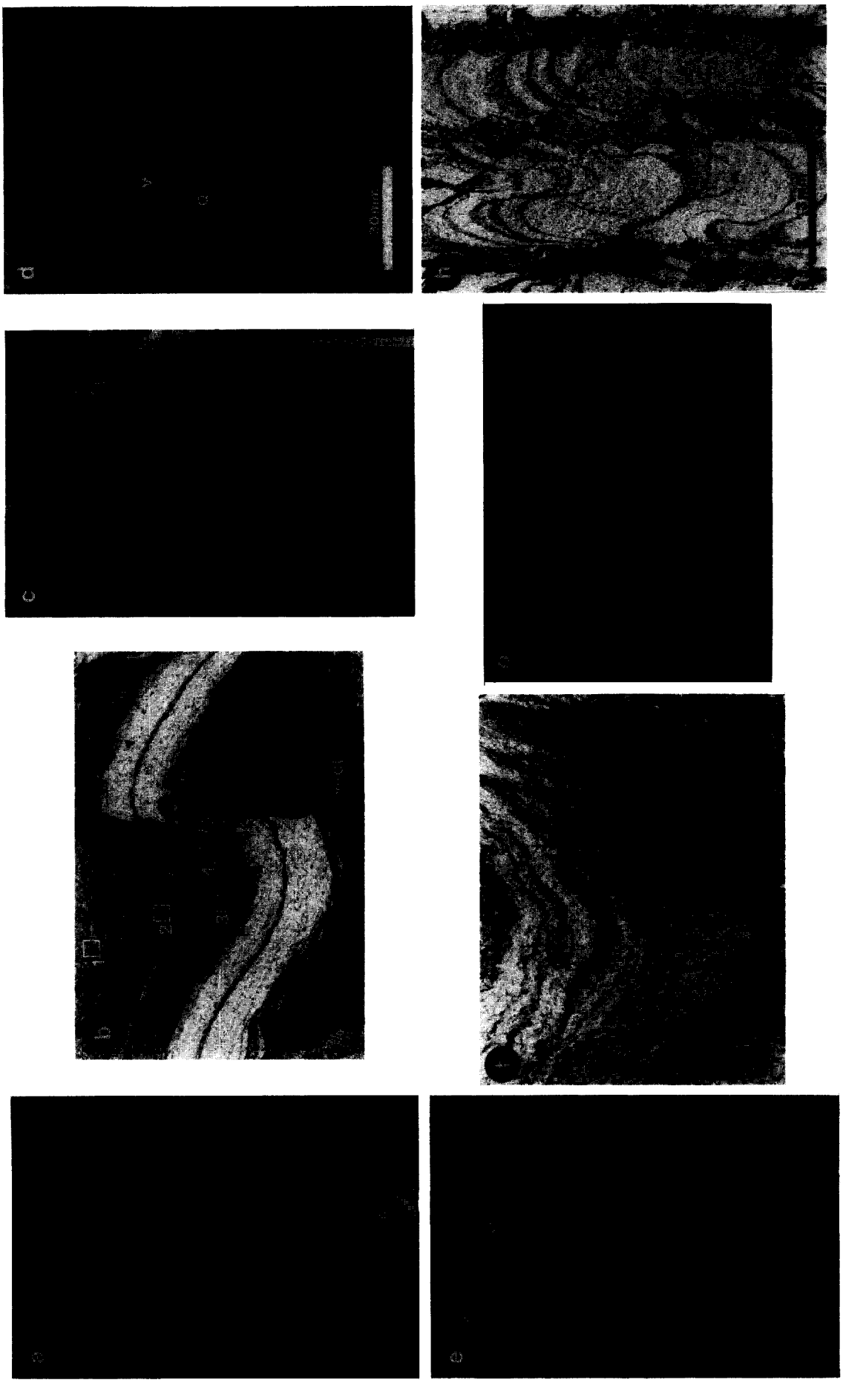

Fig. 4. Meso- and microscopic structures from the Songpan–Garzê Fold Belt and Wenchuan–Maowen Shear Zone. (a) Upright, tight F_1 folds in Triassic sandstones from the central portions of the Songpan–Garzê Fold Belt. (b) Microscopic asymmetric F_2 fold in chlorite zone schist to the west of the Xuelongbao Granite. The S_2 crenulation cleavage varies from stage 1 (box 1) of Bell and Rubenach (1983)'s cycle to stage 4 (box 4). Thick cleavage seams (cl) developed through pressure solution processes have resulted in dissolution of quartz from the short limb of the asymmetric F_2 fold. (c) Open, asymmetric F_2 folds with weak development of an S_2 crenulation cleavage in biotite grade schist. (d) Domainal S_2 cleavage and asymmetric F_2 folds in garnet–biotite schist. Symbols: Q = quartz-rich microlithon, M = mica-rich cleavage domain. (e) Isoclinally folded quartz vein (f_2) in pervasively foliated (S_2) garnet–biotite schist. Lens cap is approximately 50 mm in diameter. (f) Microstructural variations in S_2 crenulation cleavage development from garnet–biotite schist. See Fig. 6 for location with respect to a small asymmetric F_2 fold. See text for discussion of the stages of cleavage development represented in boxes 2, 4, 5 and 6. (g) Mineral elongation lineation (L_{3r}) on S_{2-3} foliation surface in D_3, high strain zone. Lineation defined by oxidized pyrite and biotite. (h) The D_{3p} crenulation (S_{3p}) of a domainal S_2 cleavage in garnet–biotite schist. Offset associated with the discrete S_{3p} cleavage indicates a reverse shear sense (section is looking toward the southwest).

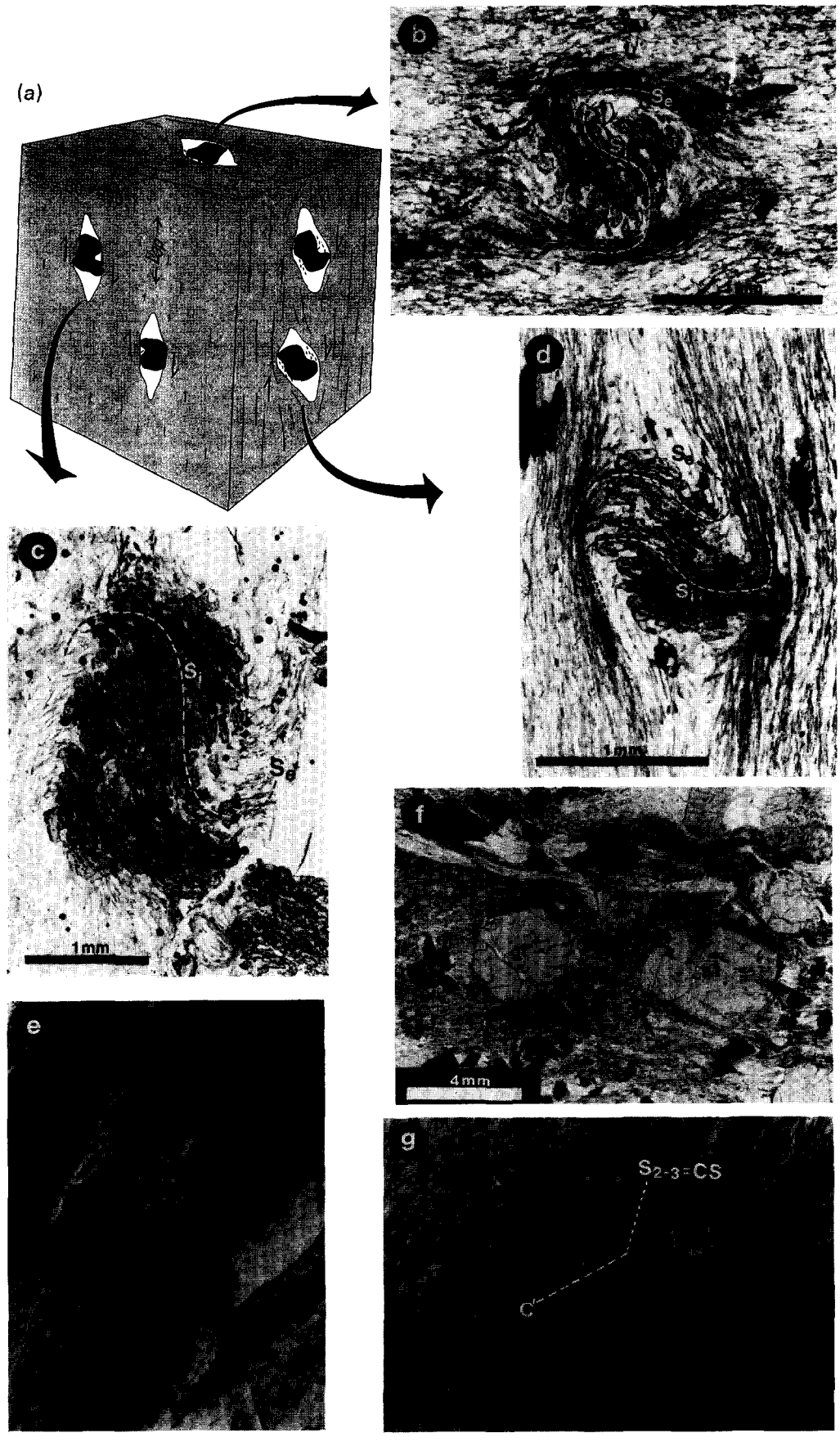

Fig. 5. Meso- and microscopic structures from the Wenchuan–Maowen Shear Zone. (a) Schematic block diagram of garnet–biotite schist with rotated garnet porphyroblasts indicating the position of the orthogonal thin sections. (b) Photomicrograph of a rotated garnet porphyroblast cut perpendicular to S_{2-3} and perpendicular to L_{3p} (h-section). Note how the internal foliation (S_i) has a smooth sinusoidal shape and is continuous with the external foliation ($S_e \equiv S_{2-3}$). (c) Photomicrograph of a rotated garnet porphyroblast cut parallel to S_{2-3} and parallel to L_{3p} (l-section). (d) Photomicrograph of a rotated garnet porphyroblast cut perpendicular to S_{2-3} and parallel to L_{3p} (v-section). (e) Asymmetric F_{3r} folds from a retrogressed D_{3r} high strain zone adjacent to the Wenchuan–Maowen Fault. (f) Staurolite–garnet–biotite schist from the west of Shapai. Main fabric is an S_{2-3} composite foliation resulting from the reactivation of S_2 during D_{3p}. The porphyroblast-rich nature of the schist during the D_{3p} shear has resulted in significant microscopic strain partitioning. This has led to crenulation of the fabric (cr) in porphyroblast pressure shadows and the development of a planar high strain S_{2-3} foliation elsewhere. Symbols: (gt) = late garnet porphyroblast, (st) = staurolite porphyroblast wrapped by S_{2-3}. (g) The S–C' fabric at the western margin of Proterozoic basement, near Shapai. Photograph is taken looking toward the north and shear sense is west-over-east.

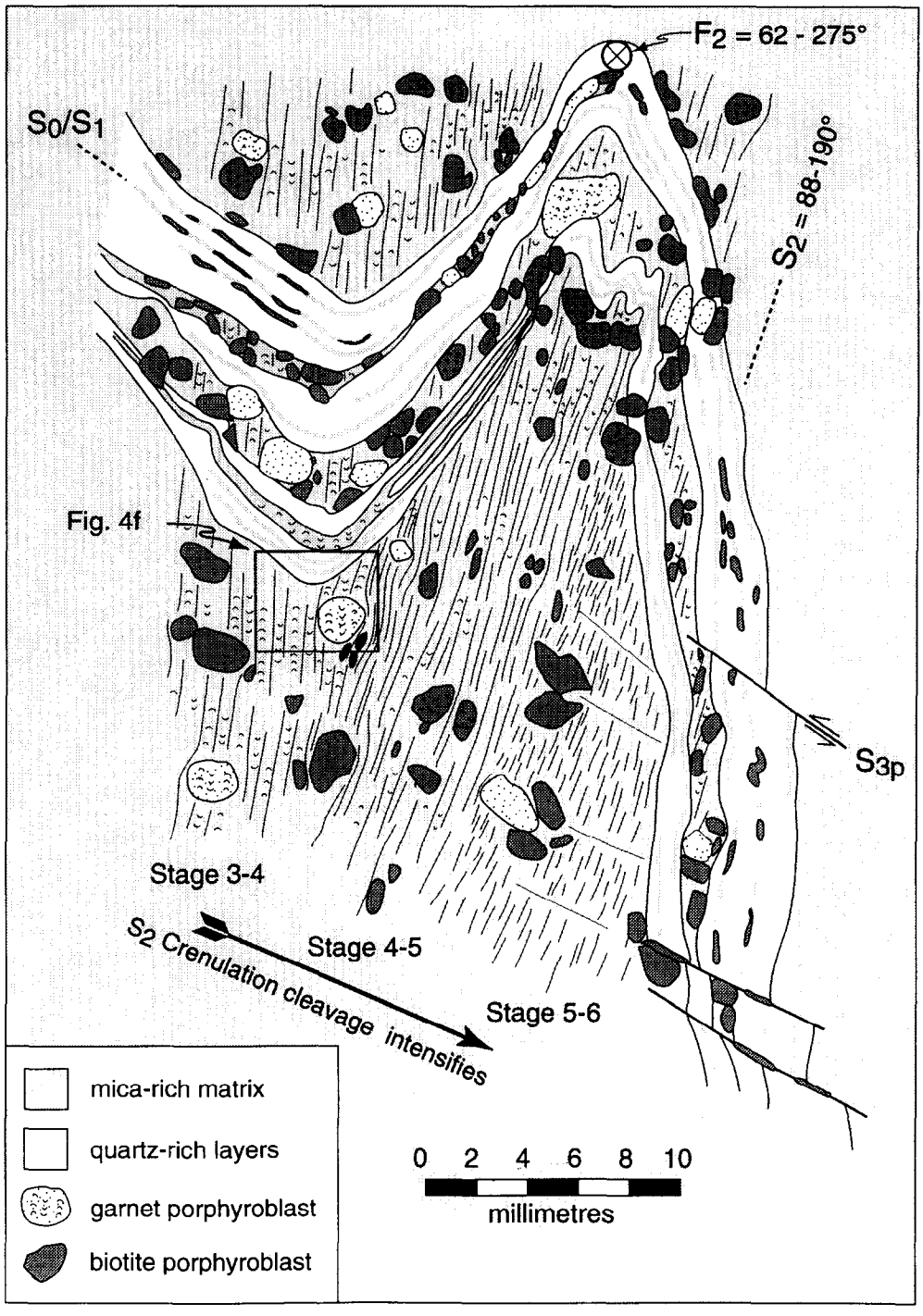

Fig. 6. Sketch of a microscopic F_2 fold in garnet–biotite schist. The fold exhibits sinistral asymmetry and the axial surface S_2 crenulation cleavage intensifies toward the long limb of the fold. The stages of the crenulation cleavage development are after Bell and Rubenach (1983). Many of the garnet and biotite porphyroblasts preserve earlier stages of the cleavage development as crenulated inclusion trails with axial surfaces parallel to S_2. The D_{3p} deformation is represented by a discrete S_{3p} crenulation cleavage oblique to S_2 and exhibiting a reverse shear sense.

asymmetric F_2 fold. In this example, the extent of the partitioning is less extreme than in the lower grade metamorphic rocks. This may be due to the predominance of crystal plastic deformation mechanisms at upper greenschist facies conditions compared to fluid controlled mechanisms such as pressure solution operating at lower metamorphic grades (Gray & Durney 1979).

The orientation of S_2 varies systematically across the shear zone, with strike rotating from east–west to northeast–southwest with increasing strain (Fig. 3). However, the S_2 fabric is deflected around the Xuelongbao Granite and is generally parallel to the margin within 1–2 km of the pluton. This change in the geometry of S_2 with respect to the margins of the shear zone is similar to that observed in many mesoscopic ductile shear zones where the foliation originally develops perpendicular to the principal finite shortening direction or at 45° to the shear direction (Ramsay & Graham 1970). This fabric is then progressively rotated into the shear

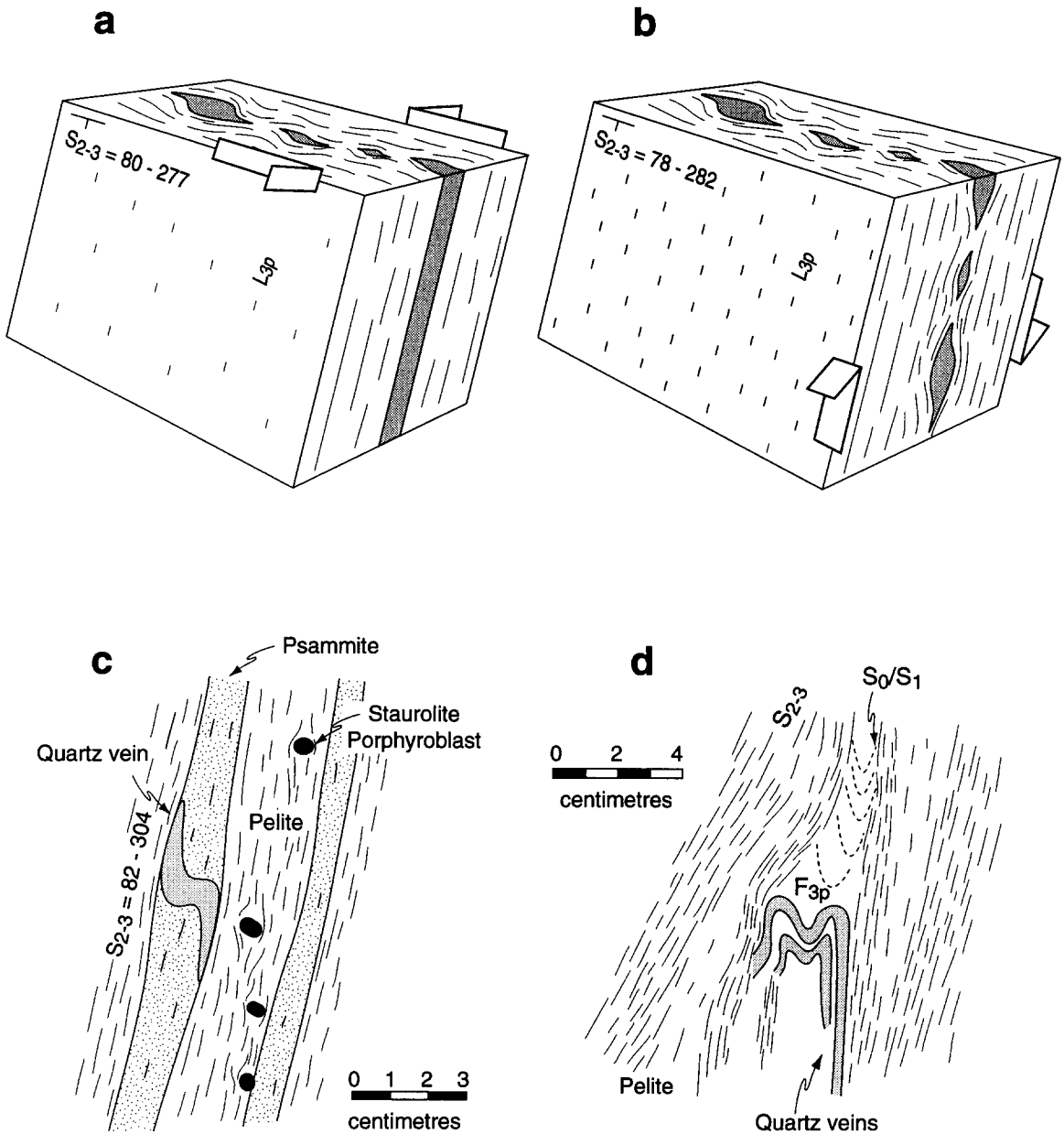

Fig. 7. Sketches of mesoscopic field relationships from the Wenchuan–Maowen Shear Zone. (a) Semi-schematic block diagram of an outcrop showing the horizontal boudinaging of quartz veins during D_2 and the weakly developed, conflicting L_{3p} mineral elongation lineation. This relationship is typical of many outcrops in the western half of the Wenchuan–Maowen Shear Zone. (b) Semi-schematic block diagram of an outcrop which has experienced relatively high D_3 strain. The L_{3p} lineation is much stronger than in (a) and boudinaging of the quartz vein is apparent in both the horizontal (D_2) and vertical (D_{3p}) sections. (c) Field sketch of a strongly asymmetric F_{3p} folded quartz vein in staurolite grade schist to the west of Shapai. The S_{2-3} is strongly developed in the pelites as a result of lithologically dependent partitioning of the D_{3p} strain. (d) Field sketch of kyanite grade schist with sub-horizontal F_{3p} folds preserved between mesoscopic D_{3p} high strain zones represented by the intense S_{2-3} foliation. Preservation of the S_1 fabric indicates that these folds developed in a region where S_1 and S_2 were not parallel, i.e. the hinge zone of a macroscopic F_2 fold.

direction, i.e. parallel to the margins of the shear zone, in this case northeast–southwest.

At high D_2 strain, quartz veins in competent lithological (i.e. psammitic) layers are commonly boudinaged in a subhorizontal direction (Fig. 7a). The sub-horizontal boudinage and steeply plunging F_2 fold axes indicate a sub-horizontal extension or shear direction, i.e. transcurrent shear. A sinistral shear sense during D_2 is evidenced by the consistent sinistral asymmetry of meso- and microscopic F_2 folds (Figs. 4b–d and 6) and boudins (Fig. 7a) and the macroscopic sinistral rotation of S_0, S_1 and S_2 from the fold belt into the shear zone. A down-dip mineral elongation lineation (Fig. 4g) which is developed throughout much of the shear zone is inconsistent with the kinematic history indicated by the other D_2 structures (Fig. 7a). Consequently, this lineation is attributed to reactivation of the S_2 fabric during D_3 deformation.

D_3

The third phase of deformation (D_3) encompasses a range of co-planar and co-linear ductile to semiductile structures which developed in response to reverse shear

within the Wenchuan–Maowen Shear Zone. Despite the similar orientation and kinematics of D_3 structures, they are further sub-divided into two distinct groups on the basis of the metamorphic conditions during formation. Ductile folds and fabrics associated with prograde–peak mineral assemblages are defined as D_{3p} structures, whilst D_{3r} structures are ductile–semi-ductile in nature and associated with retrogression of the peak paragenesis.

D_{3p} structures include a spaced cleavage, defined by the alignment of sub-parallel muscovite and biotite (S_{3p}), which crenulates S_2 (Figs. 4h and 6), but progressive overprinting as observed with the D_2 crenulation overprinting of S_1 is not recorded. In fact, parallelism of the bulk shear plane between D_2 and D_{3p}, apparently controlled by the margins of the shear zone and particularly the steep orientation of the Wenchuan–Maowen Fault, has resulted in ubiquitous reactivation of S_2 and the formation of a composite foliation referred to hereafter as S_{2-3}. Due to the reactivation and formation of a composite fabric, it is not possible to distinguish between D_2 and D_3 deformation on the basis of overprinting foliations; instead, variations in the style and orientation of the linear structures are used. The D_{3r} deformation, also co-planar to D_{3p} and D_2, was restricted to localized high strain zones. While D_{3r} shear within these high strain zones continued to be accommodated by the S_{2-3} fabric, semi-ductile structures such as S–C' fabrics and kink folds were also developed.

L$_3$ *lineations*. The down-dip mineral elongation lineation (L_{3p}), developed throughout much of the shear zone, is variably defined by elongate quartz ribbons and aligned muscovite, biotite and staurolite, depending upon metamorphic grade. This lineation first appears in relatively low D_{3p} strain regions where it is orthogonal to the extension direction indicated by sub-horizontal boudinage of quartz veins (Fig. 7a). However, with increasing D_{3p} strain, the L_{3p} lineation increases substantially in intensity and boudinage of quartz veins becomes increasingly apparent in vertical as well as horizontal sections. Within the D_{3r} high strain zones the lineation (L_{3r}) is further intensified, but is now defined by elongate quartz, oxidation spots or by an alignment of muscovite and chlorite.

Four principal F_3 fold styles have developed in response to variations in temperature, strain and the orientation of pre-existing fabrics. The first three fold styles are F_{3p} folds developed during the prograde D_{3p} deformation, while the fourth set are F_{3r} folds related to D_{3r} high strain zones.

F$_{3p}$ *folds*. These are similar in appearance to F_2 folds, but can be confidently identified, even when overprinting relations are not observed, by the consistent sub-horizontal orientation of the axes (cf. the steep plunge of F_2, Fig. 3). Although rare, there are three styles of folds which developed during the prograde D_{3p} deformation, all of which exhibit a consistent asymmetry indicating reverse shear, equivalent to the quartz boudins.

(1) Asymmetric microfolds associated with the discrete S_{3p} crenulation cleavage. These folds are restricted to the low strain, western portion of the Wenchuan–Maowen Shear Zone, and are specifically developed where S_2 is steeply dipping to the southeast and is therefore not in a favourable orientation for reactivation.

(2) Strongly asymmetric fold hinges in quartz veins (Fig. 7c). These are predominantly preserved in psammites and are the result of partitioning of the D_{3p} shear strain into the pelitic layers. Where $S_0/S_1/S_2$ are parallel to the margins of the shear zone, and hence the bulk shear plane, they have been reactivated to form the composite S_{2-3} foliation. However, D_2 or early D_{3p} quartz veins within more competent lithologies, which are not completely transposed into the early fabrics, are involved in this style of folding.

(3) Tight to isoclinal meso- to macroscopic folds with axial surfaces parallel to the overall S_{2-3} orientation. Once again, these folds are mainly developed in quartz veins, but occasional tight folding of S_0/S_1 is observed (Fig. 7d). Such folds are developed in regions where S_0/S_1 and S_2 are not parallel (i.e. in the hinge zones of macroscopic F_2 folds).

F$_{3r}$ *folds*. These are asymmetric, semi-ductile kink folds with axial surfaces dipping steeply to the E (Fig. 3) and are common in the D_{3r} high strain zones, particularly in the Silurian schist adjacent to the Xuelongbao Granite and Wenchuan–Maowen Fault (Fig. 5e).

The nature of the F_3 folds, extensive distribution of the mineral lineation and co-planarity of D_2 and D_3 indicate the importance of the partitioning of D_3 shear strain and reactivation of the S_2 foliation at a mesoscopic scale during D_3 deformation. These processes have also been significant at a microscopic scale resulting in the formation of a characteristic range of microstructures.

Garnet inclusion trails

In garnet–biotite schist, with a strong L_{3r} mineral lineation, garnet porphyroblasts exhibit smooth sinusoidal inclusion trails (S_i) which are continuous with the external foliation ($S_e \equiv S_{2-3}$) (Figs. 5a–d). The significance of such inclusion trails and the question of whether they indicate rotation of porphyroblasts relative to an external reference frame has been a topic of intense debate over recent years (see Bell *et al.* 1992 and Passchier *et al.* 1992 for summaries of both sides of the rotation debate). Recognition of the co-planarity of D_2 and D_3 deformation leads to the unequivocal conclusion that sinusoidal inclusion trails which are continuous with the S_{2-3} fabric are the result of rotation of the porphyroblasts rather than rotation of micaceous matrix during orthogonal deformations. In addition, non-rotation of the matrix means that the shear sense determined from the rotated garnets is with respect to an external refer-

ence frame, rather than simply relative rotation with respect to the rotating matrix (cf. Visser & Mancktelow, 1992). Orthogonal sections cut perpendicular to S_{2-3} and L_{3r} (Fig. 5b), parallel to S_{2-3} and L_{3r} (Fig. 5c), and perpendicular to S_{2-3} and parallel to L_{3r} (Fig. 5d) were examined. Garnets from all three sections show evidence of rotation which allows us to place some constraints on the nature and direction of shear during garnet growth.

Horizontal sections cut perpendicular to S_{2-3} and L_{3r} (h-sections, Fig. 5b) exhibit relatively smooth sinusoidal inclusion trails from core to rim indicative of sinistral or anticlockwise rotation. Garnets from sections perpendicular to S_{2-3} but parallel to L_{3r} (v-sections, Fig. 5d) typically have straight inclusion trails in their cores but distinctly sinusoidal trails in the outer half of the porphyroblasts. Many garnets from sections parallel to both S_{2-3} and L_{3r} (l-sections, Fig. 5c) do not exhibit inclusion trails, but the significant number which do, have long straight inclusion trails in their cores curving into the S_e orientation toward the outer margins of the porphyroblasts. The curvature of inclusion trails from v- and l-sections indicate a component of dextral or clockwise shear in both cases. The only assumption necessary for interpreting the three-dimensional geometry of the inclusion trails and subsequently the kinematics of shear during garnet growth has already been justified, i.e. that due to the co-planar nature of D_2 and D_3 the external foliation in the matrix was not rotated during garnet growth. Following this assumption, the situation can be envisaged as similar to the classical case of shear-induced rotation of a porphyroblast overgrowing a fixed external foliation as originally documented by Powell & Treagus (1969, 1970) and Rosenfeld (1970) and more recently by Gray & Busa (1994). In these previous studies, the porphyroblast rotation axis (R) maintains a constant orientation parallel to the plane of shear and perpendicular to the shear direction. However, in the case described here, sinusoidal inclusion trails indicating rotation are present in h-, v- and l-sections, and garnet growth is thought to have occurred during two progressive coplanar but non-co-linear deformations. Hence, it is important to determine if R and the garnet also rotated on an axis perpendicular to the plane of shear.

To evaluate the significance of the three-dimensional geometry of the observed inclusion trails, we will discuss firstly the inclusion trails predicted for three possible deformation–time (D–t) paths which are based on mesoscopic observations of the foliations, folds, lineations and boudinage development. It is also necessary to consider two endmember scenarios of how the porphyroblast and rotation axis R rotate perpendicular to the shear plane. Scenario (a): in response to changes in the external shear direction, the entire garnet porphyroblast and R rotate simultaneously on an axis perpendicular to the shear plane, so that the porphyroblast itself remains coaxial to the deformation. Scenario (b): where R rotates in response to the changing shear direction but the garnet does not, resulting in rotation of R relative to the garnet's frame of reference.

Deformation–time path (i). The deformation takes the form of two distinct co-planar but orthogonal phases of shear, D_2 = sinistral and D_3 = reverse. Rotation scenario (a) is not relevant to this situation, as it involves orthogonal overprinting phases of deformation and the porphyroblast is only likely to rotate around an axis perpendicular to the shear plane in response to a progressive rotation of the shear direction. Rotation scenario (b) would produce trails with straight cores and sinusoidal rims in sections parallel to the direction of final shear, e.g. v-sections, while sections parallel to the early shear direction (h-sections) will have sinusoidal trails in the cores, truncated by straight trails in the rims (Fig. 8a). Sections parallel to the shear plane will also have sinusoidal cores and straight trails in the rims, but the final geometry visible in these sections will be strongly dependent upon the amount of rotation during the final shearing event.

Deformation–time path (ii). Garnet growth occurred during a single period of oblique shear which was subsequently overprinted by a phase of reverse shear during which the down-dip lineation developed. As for D–t path (i), the first rotation scenario is not applicable to this situation. Rotation scenario (b) will result in inclusion trails from all three sections having sinusoidal geometries from core to rim, but rotation of the garnets parallel to the lineation direction, following cessation of their growth, means that in all cases S_i will be truncated by S_e (Fig. 8b).

Deformation–time path (iii). The sinistral and reverse shear of D_2 and D_3 are end members of a progressive transpressional episode of deformation during which the shear direction, and hence R, rotated through approximately 90° parallel to the shear plane. Rotation scenario (a) is plausible for this D–t path; however, if the porphyroblast remains coaxial to the deformation, then sinusoidal inclusion trails would be visible only in sections parallel to the last direction of shear (i.e. v-sections). For rotation scenario (b), where R has been rotated in response to a progressive change in the shear direction, porphyroblasts from all three sections will exhibit sinusoidal inclusion trail geometries. However, trails from sections cut parallel to the lineation should include straight portions in the core of the porphyroblasts and the proportion of straight to sinusoidal trail will increase from v- to l-sections (Fig. 8c).

The observed inclusion trail geometries (Figs. 5a–d) bear a remarkable resemblance to those predicted by rotation scenario (b) and for D–t path (iii) (Fig. 8c), indicating that garnet growth occurred during an episode of progressive transpressional deformation of which D_2 strike-slip and D_3 reverse shear are end members. It also shows that while the garnet porphyroblasts only rotated about a single axis (R), this axis progressively rotated within the shear plane to remain perpendicular to the shear direction.

Microscopic partitioning of D_3 strain is evident particularly in high strain, porphyroblast-rich, staurolite

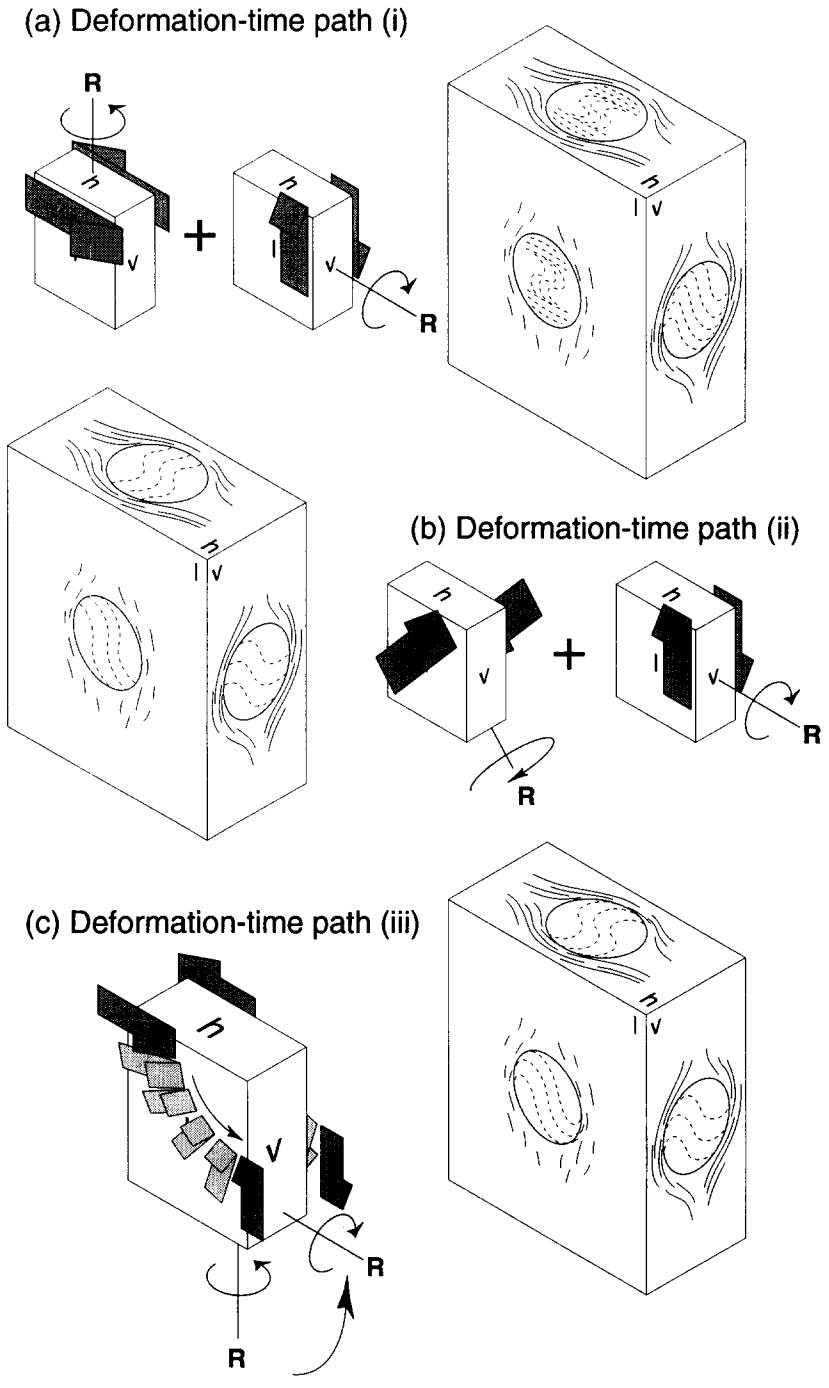

Fig. 8. Cartoons illustrating inclusion trails in garnet porphyroblasts predicted for different deformation–time paths (i)–(iii). (a) Two co-planar but orthogonal phases of shear with the rotation axis (R) parallel to either a horizontal (h) or vertical plane (v). (b) Garnet growth during oblique shear overprinted by post-porphyroblast growth reverse shear. (c) A progressive change from sinistral shear (parallel to h) to reverse shear (parallel to v). See text for detailed discussions of the deformation–time paths.

and kyanite grade schists to the southwest of the Xuelongbao Granite. An extremely anisotropic mica-rich matrix contains a complex mosaic of porphyroblasts, crenulations and planar foliations which have developed in response to partitioning of the strain (Fig. 5f). Microscopic crenulations of S_{2-3} (cr in Fig. 5f) with axial surfaces at a low angle to the overall fabric have developed in the pressure shadows of some porphyroblasts while in adjacent regions a relatively planar, high strain foliation (S_{2-3}) is evident. Staurolite porphyroblasts have distinct pressure shadows and are commonly wrapped by the high strain S_{2-3} fabric (st in Fig. 5f), while garnet growth appears to be relatively late in the deformation history and has had little effect on the partitioning of deformation in the matrix (gt in Fig. 5f).

PROGRESSIVE LOCALIZATION OF D_3 STRAIN AND THE DEVELOPMENT OF D_{3r} HIGH STRAIN ZONES

Although the D_3 event has affected a zone approximately 15–20 km wide (as illustrated by the extent of the down-dip stretching lineation), progressive localization

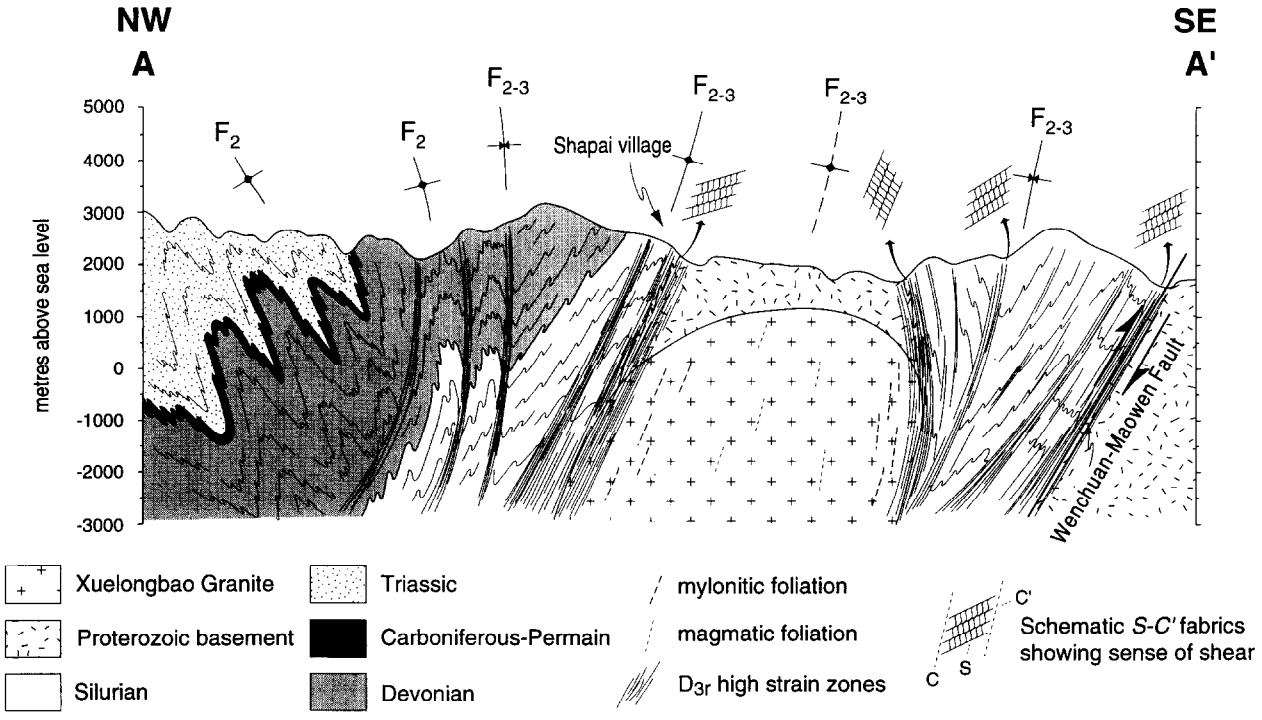

Fig. 9. Cross-section A–A′ from the west of Shapai to the Wenchuan–Maowen Fault. The F_{2-3} folds are F_2 structures reactivated during D_{3p}. The nature of the D_{3r} high strain zones at depth is based on the lateral continuity of these zones and the observed widening of these zones with increasing temperature.

of the deformation has resulted in the formation of sub-planar D_{3r} high strain zones up to 1.3 km in width. The most commonly developed folds in these high strain zones are the F_{3r} asymmetric semi-ductile kink folds (Fig. 5e) described earlier. Within many of these high strain zones, especially in mica-rich lithologies and in the margins of the Xuelongbao granite and granites of the Proterozoic basement, discrete shear surfaces have formed at an angle of 30–45° to the S_{2-3} foliation (Figs. 5g and 9). Although the history of this S_{2-3} fabric is complex, including reactivation during progressive co-planar deformations, its parallelism to the margins of the shear zone and hence bulk shear plane means that it has accommodated the majority of the strain and is hence essentially equivalent to the high strain *CS* fabric of Berthé *et al.* (1979). In contrast, only minor movement appears to have occurred on the discrete shear surfaces and these are interpreted as *C′*-surfaces (Blenkinsop & Treloar 1995) equivalent to extensional crenulation cleavage of Platt and Vissers (1980). The combined structure, termed an *S–C′* fabric after Blenkinsop & Treloar (1995), is useful as a kinematic indicator in the same way as a classical *S–C* fabric. In all of these high strain zones, the sense of shear from the *S–C′* fabrics is reverse or West-over-East. The *S–C′* fabric in the Xuelongbao Granite is transitional into a high temperature mylonitic foliation which is observable for up to 2 km in from the granite margins. This high temperature deformational fabric then decreases in intensity toward the centre of the intrusion which is essentially undeformed and exhibits a weak magmatic foliation.

METAMORPHISM

The greater part of the Songpan–Garzê Fold Belt is composed of a thick sequence of Triassic turbidites metamorphosed to lower greenschist facies. Typical assemblages include white mica + chlorite + quartz + albite ± pyrite ± graphite. Upper greenschist–amphibolite facies schists are confined to the high strain regions at the margins of the fold belt, such as the Wenchuan–Maowen Shear Zone and the Deixi Fault, described by Dirks *et al.* (1994). Within the central Longmen Shan, regional metamorphic biotite, garnet, staurolite and kyanite isograds are generally sub-parallel to the boundaries of the Wenchuan–Maowen Shear Zone, but are locally deflected by the Xuelongbao Granite and cross-cut by the D_{3r} high strain zones (Fig. 10). Highest grades of metamorphism were reached in the kyanite zone, to the southwest of the Xuelongbao Granite. Average pressure–temperature calculations (Powell & Holland 1994) using the thermodynamic data set and THERMOCALC program of Powell & Holland (1988) and comparisons with published petrogenetic grids (Powell & Holland 1990, Xu *et al.* 1994) indicate that peak kyanite + staurolite + plagioclase + biotite + muscovite + graphite assemblages equilibrated in the upper limits of the staurolite + biotite field in KFMASH at approximately 600°C and 10 kbar.

Across the Wenchuan–Maowen Shear Zone, there is a progressive relationship between regional metamorphic porphyroblastesis and foliation development. At the western margin of the shear zone, where D_2 strain is

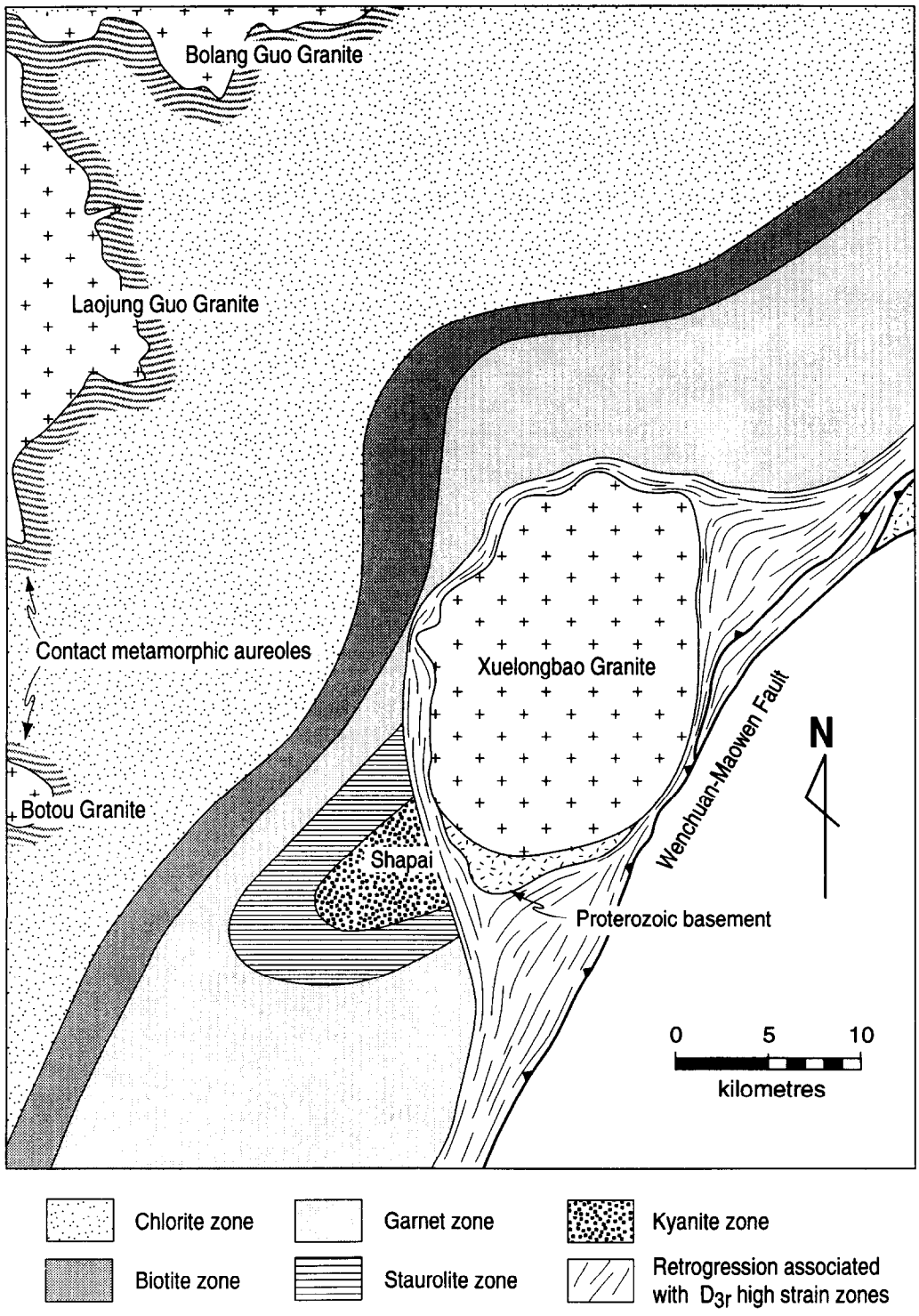

Fig. 10. Map of the Xuelongbao region showing the distribution of the regional metamorphic isograds, contact metamorphic aureoles and retrograde D_{3r} high strain zones.

relatively low, S_1 is defined by fine-grained (<1 mm) muscovite which is overgrown by a coarser (<2 mm) phase of muscovite and biotite, which define S_2. Straight and sinusoidal inclusion trails of quartz and graphite, at a high angle to S_2, within these biotites indicate growth during progressive crenulation of S_1 (Bell & Rubenach 1983). In high D_2 strain regions, biotite, garnet and occasionally plagioclase porphyroblasts preserve quartz and graphite inclusion trails indicative of porphyroblast growth during stages 4–6 of schistosity formation via a crenulation cleavage (Figs. 4f and 6), and S_1 (where present) is locally defined by biotite. To the north of the Xuelongbao Granite, garnet porphyroblasts occasionally overgrow D_3 crenulations while others record evidence of a progressive D_2–D_{3p} transpressional deformation (Figs. 5a–d). In the staurolite and kyanite zones to the south of the granite, the index minerals variably overgrow microscopic crenulations of S_{2-3} and are wrapped by the same S_{2-3} fabric (Fig. 5f). Timing relationships between porphyroblast growth and the

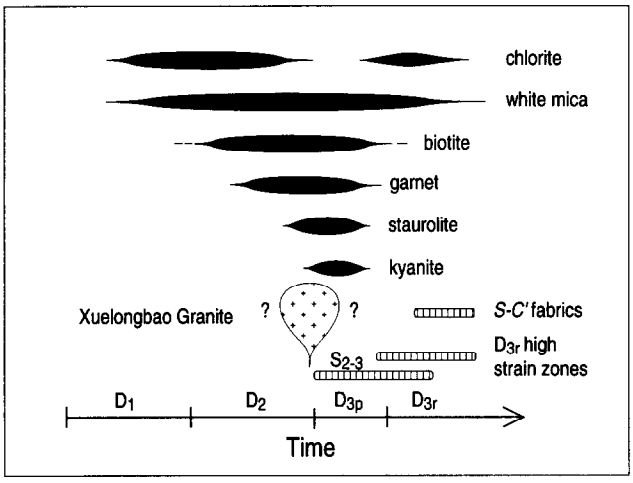

Fig. 11. Schematic metamorphism vs deformation diagram showing the timing of porphyroblast growth relative to the important structural and magmatic events.

development of the various tectonic fabrics are illustrated in Fig. 11. In summary, the high-grade metamorphism characterized by garnet + biotite and kyanite + staurolite assemblages post-dates the original crustal thickening event (D_1) with peak conditions occurring from late D_2 to D_{3p}. The kinematics of D_{3p} shear suggest that peak metamorphism is coincident with the initiation of tectonically driven exhumation. These relative timing relationships are characteristic of Barrovian-type metamorphic terranes, where heating is considered to be the conductive response of the lithosphere to deformation [i.e. tectonic burial (D_1)]. In such cases, peak metamorphism is separated from the thickening event by a timespan corresponding to the lengthscale of the equilibrating lithosphere, typically on the order of tens–one hundred million years (England & Thompson 1984), and uplift is an erosion driven isostatic response to the lithospheric thickening (England & Richardson 1977).

Stratigraphic constraints in the Longmen Shan and Western Sichuan Foreland Basin (Chen *et al.* 1994, 1995, Dirks *et al.* 1994, Worley *et al.* 1994) indicate that significant uplift and erosion of the Songpan–Garzê Fold Belt was underway by the end of the Late Triassic (Rhaetian). This suggests that tectonic exhumation was initiated and peak metamorphic conditions obtained within < 15 Ma of the initiation of the Indosinian Orogeny. Therefore, although the metamorphism within the Wenchuan–Maowen Shear Zone appears to have been a Barrovian-type, either a contribution from an advective heat source is required or the timescales for conductive thermal equilibration are much shorter than the numerically derived results of England & Thompson (1984) indicate.

RETROGRESSION ASSOCIATED WITH D_3 HIGH STRAIN ZONES

The Fe–Mg aluminosilicate phases in the regional metamorphic assemblages are partially to completely retrogressed to an assemblage of muscovite + chlorite ± biotite in the D_{3r} high strain zones (Fig. 10). The strong alignment of mica and quartz in the down-dip stretching lineation developed on the S_{2-3} fabric illustrates that recrystallization was synchronous with the D_{3r} reverse shear. This D_{3r} thrusting in the margin of the fold belt has been equated with the initiation of the nappes within the Longmen Shan Thrust–Nappe Belt at the end of the late Triassic (T_{3x}) (Chen *et al.* 1995).

The kinematics of the D_{3r} high strain zones and their extensive retrogression to lower greenschist facies indicates that reverse shear along these zones resulted in tectonic exhumation of the Wenchuan–Maowen Shear Zone. Localisation of retrogressing fluids into the high strain zones during tectonic exhumation suggests two likely fluid sources: (1) they could represent hydrothermal circulation cells set up in response to the thermal perturbation caused by rapid exhumation of hot, mid–lower crustal rocks in the hanging wall of the Wenchuan–Maowen Shear Zone (cf. Koons 1987); (2) the high strain zones may have behaved as fluid conduits during tectonic exhumation of the fold belt, for fluids originating from lower crustal dehydration reactions during ongoing orogenesis. This implies that deformation and metamorphism of the fold belt was continuing at depth during tectonic exhumation, a situation similar to that proposed by Koons (1990) and Norris *et al.* (1990) for the transpressional Alpine Fault orogen in the South Island of New Zealand.

THE XUELONGBAO GRANITE

Clear contact metamorphic aureoles occur around all of the Indosinian granites in the fold belt, apart from the Xuelongbao Granite (Fig. 10). Typical contact metamorphic porphyroblasts in these aureoles include biotite, andalusite and cordierite, but not sillimanite; migmatites are not developed. Dirks *et al.* (1994) suggest that pressure was approximately 3–4 kbar and temperature did not exceed 650°C during the formation of the aureoles. Although the maximum regional metamorphic conditions within the shear zone are spatially associated with the Xuelongbao Granite, there is no evidence of a contact metamorphic aureole associated with this intrusion. In fact the contact between the Xuelongbao Granite and the schists is a D_{3r} high strain zone, affecting both the granite and schist, where the regional metamorphic assemblages have been retrogressed to the chlorite zone. The recognition of this zone of high strain and retrogression at the margins of the granite brings into question the age and significance of the Xuelongbao Granite with respect to the structural and metamorphic evolution of the shear zone.

Historically, the Xuelongbao Granite has been mapped as a fault-bounded Proterozoic basement complex (Li *et al.* 1975a,b, Long 1991). This conclusion was probably based on the deformed nature of the granite margin and lack of a contact aureole. However, detailed

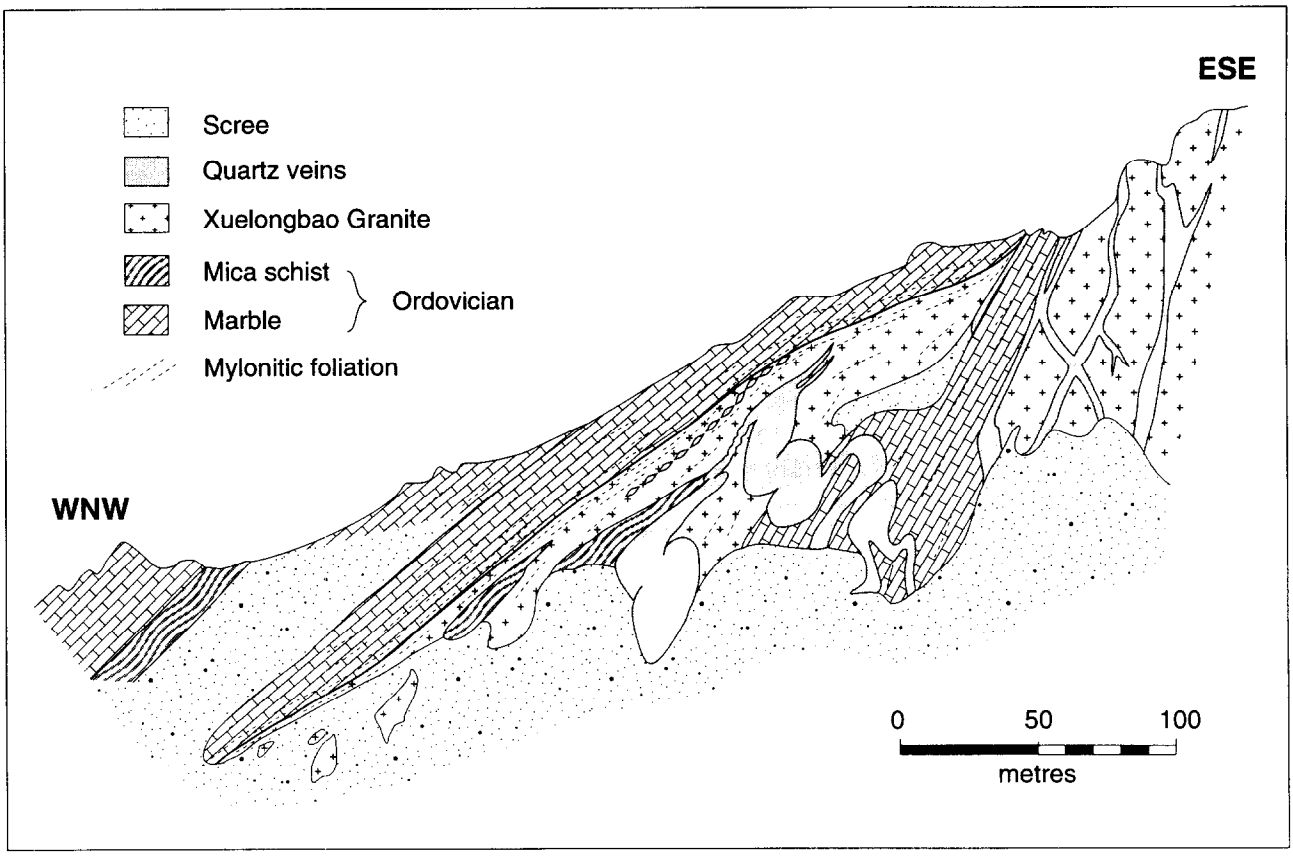

Fig. 12. Field sketch of part of the western margin of the Xuelongbao Granite. Note the presence of both marble and mica schist rafts within the granite giving a maximum age of Latest Ordovician. The D_{3p}–D_{3r} deformation is illustrated by mylonitization of both the marble and granite within 50 m of the contact, and the folded quartz veins. The quartz veins probably formed early during D_{3r} as a result of the high fluid flow along the contact and were subsequently deformed in response to continuing D_{3r} shear during tectonic exhumation.

observations of the highly strained western margin of the granite (Fig. 12) reveal that large rafts of the Palaeozoic sedimentary sequence were entrained during emplacement. Hence intrusion of the Xuelongbao Granite must at least post-date the deposition of these sediments (Ordovician). Development of D_{3r} high strain zones along the granite margin, including a mylonitic foliation within the granite parallel to S_{2-3} in the country rocks and D_3 folding (up to 50 m wavelength) and boudinaging of quartz veins, constrains the minimum age of the emplacement to pre-D_{3r}.

Partitioning of D_{3r} strain along the granite-schist contacts resulting in the ubiquitous formation of retrogressed D_{3r} high strain zones means that any contact metamorphic aureole associated with the Xuelongbao Granite, and hence the essential timing relations preserved herein, have been destroyed. It is therefore extremely difficult to constrain accurately the timing of intrusion and the majority of evidence available at this stage is relatively circumstantial. The numerous other granite plutons intruded at high levels in the Songpan–Garzê Fold Belt cross-cut D_1 structures and have radiometric ages ranging from ~205–150 Ma (Zhang *et al.* 1991), indicating a general relationship between the Indosinian Orogeny and granite magmatism.

With a timing of Xuelongbao Granite emplacement coincident with progressive D_2–D_{3p} deformation, it is important to consider the resulting thermomechanical effects of granite emplacement on the shear zone. Once again, direct observation of these effects is complicated by post-emplacement D_{3r} shear, as the amphibolite facies rocks have probably been emplaced into their present position relative to the intrusion from lower crustal levels. However, migration of large quantities of granite magma up through the transpressional shear zone is likely to result in the introduction of advective heat. Two possible effects of additional advective heat are: (1) increasing the thermal gradient to enable the attainment of peak metamorphic conditions <15 Ma after the onset of orogenesis; (2) thermal softening and subsequent partitioning of deformation into the region experiencing elevated temperatures. Evidence of this effect may be the high D_{3p} strain evident in the staurolite to kyanite grade rocks near Shapai. The granite continued to control the partitioning of deformation within the shear zone during D_{3r} exhumation. Following crystallization, the strength of the granite would be significantly greater than that of the foliated schist, hence resulting in the intrusion behaving as a relatively rigid body during exhumation. Hence, D_{3r} shear would be partitioned into the granite-schist contact leading to the formation of the D_{3r} retrograde high strain zones.

CONCLUSIONS

(1) Indosinian deformation in the Wenchuan–Maowen Shear Zone evolved from SW-directed compression (crustal thickening during D_1) through sinistral transcurrent shear (accommodation of differential strain between the fold belt and Yangtze Craton; D_2) to SE-directed compression (tectonically driven uplift; D_3). Structures developed during D_3 tectonic exhumation are sub-divided into those associated with the prograde–peak mineral paragenesis (D_{3p}) and a second set of co-planar and co-linear structures developed during retrogression of the regional metamorphic assemblages. Progressive localization of deformation from D_1 to D_{3r} resulted in the preservation of overprinting relationships within the Wenchuan–Maowen Shear Zone.

(2) Co-planarity of the D_2 and D_3 deformations led to reactivation of the favourably oriented S_2 fabric. This resulted in the formation of a composite S_{2-3} foliation with a strong down-dip stretching lineation (L_3) during D_3.

Growth of garnet porphyroblasts during the co-planar deformations (D_2 and D_{3p}) indicates that the sinusoidal inclusion trails are the result of porphyroblast rotation. The three-dimensional geometry of these sinusoidal inclusion trails suggests that D_2 and D_{3p} are the strike-slip and reverse end members of an episode of progressive transpressional deformation.

(3) Peak metamorphic conditions in the Wenchuan–Maowen Shear Zone of ~600°C and 10 kbar were reached in the Shapai region to the southwest of the Xuelongbao Granite. Syn-D_{3p} growth of kyanite and staurolite indicates that peak metamorphism was coincident with the initiation of tectonically driven exhumation of the shear zone, less than 15 Ma after the original D_1 thickening event.

(4) Intrusion of the Xuelongbao Granite is post-Ordovician and pre-D_{3r}, but an accurate estimation of the timing relative to D_2 and D_3 is not possible as retrograde D_{3r} high strain zones along the granite margins have destroyed any contact aureole which might have existed. The partitioning of deformation into the granite-schist margins indicates that the granite was crystalline and behaved as a rigid body during D_{3r} exhumation. Similar high strain zones also developed along the Wenchuan–Maowen Fault as this structure represents a pre-existing zone of weakness.

(5) Retrogression associated with D_{3r} high strain zones indicates that they acted as fluid conduits during the tectonically driven exhumation. The fluids are probably either hydrothermal or metamorphic in origin and are late in the tectonic evolution of the shear zone.

Acknowledgements—This project was made possible by financial support from the Australian Research Grants Committee and the National Natural Science Foundation of China and logistical support from the Chengdu Institute of Technology. Mr Wang Gwozhi, Dr Liu Shugen and Professor Luo Zhili are thanked for their support in the field with respect to both the local geology and the language barrier. We would also like to acknowledge Dr Chen Shefa for many useful discussions concerning the geology of the eastern Songpan–Garzê Fold Belt, Longmen Shan Thrust–Nappe Belt and Western Sichuan Foreland Basin. Dave Prior and an anonymous referee are thanked for extremely thorough and constructive reviews which, together with the editorial comments from Richard Norris, greatly improved the final version of the manuscript. The first author gratefully acknowledges the financial support of an Australian Postgraduate Research Award.

REFERENCES

Bell, T. H., Johnson, S. E., Davis, B., Forde, A., Hayward, N. & Wilkins, C. 1992. Porphyroblast inclusion-trail orientation data: *eppure non son girate**! *J. metamorph. Geol.* **10**, 295–307.

Bell, T. H. & Rubenach, M. J. 1983. Sequential porphyroblast growth and crenulation cleavage development during progressive deformation. *Tectonophysics* **92**, 171–194.

Bergh, S. G. & Karlstrom, K. E. 1992. The Chaparral shear zone: deformation partitioning and heterogeneous bulk crustal shortening during Proterozoic orogeny in central Arizona. *Bull. geol. Soc. Am.* **104**, 329–345.

Berthé, D., Choukroune, P. & Jegouso, P. 1979. Orthogneiss, mylonite and non-coaxial deformation of granites: the example of the South Armorican Shear Zone. *J. Struct. Geol.* **1**, 31–42.

Blenkinsop, T. G. & Treloar, P. J. 1995. Geometry, classification and kinematics of *S–C* and *S–C'* fabrics in the Mushandike area, Zimbabwe. *J. Struct. Geol.* **17**, 397–408.

Burg, J.-P. & Chen, G. M. 1984. Tectonics and structural zonation of southern Tibet, China. *Nature* **311**, 219–223.

Butler, R. W. H. & Prior, D. J. 1988. Tectonic controls on the uplift of the Nanga Parbat Massif, Pakistan Himalayas. *Nature* **333**, 247–250.

Chen, S., Wilson, C. J. L., Luo, Z. & Deng, Q. 1994. The evolution of the Western Sichuan Foreland Basin, SW China. *J. SE Asian Earth Sci.* **10**, 159–168.

Chen, S., Wilson, C. J. L. & Worley, B. A. 1995. Tectonic transition from the Songpan–Garzê Fold Belt to the Sichuan Basin, southwestern China. *Bas. Res.* **7**, 235–253.

Davis, B. K. 1993. Mechanism of emplacement of the Cannibal Creek Granite with special reference to timing and deformation history of the aureole. *Tectonophysics* **224**, 337–362.

Davis, B. K. 1994. Synchronous syntectonic granite emplacement in the South Palmer River region, Hodgkinson Province, Australia. *Austr. J. Earth Sci.* **41**, 91–104.

Davis, B. K. & Forde, A. 1994. Regional slaty cleavage formation and fold axis rotation by re-use and reactivation of pre-existing foliations: the Fiery Creek Slate Belt, North Queensland. *Tectonophysics* **230**, 161–179.

Dirks, P. H. G. M., Wilson, C. J. L., Chen, S., Luo, Z. & Liu, S. 1994. Tectonic evolution of the NE margin of the Tibetan Plateau: evidence from the central Longmen Mountains, Sichuan Province, China. *J. SE Asian Earth Sci.* **9**, 181–192.

England, P. C. & Richardson, S. W. 1977. The influence of erosion upon the mineral facies of rocks from different metamorphic environments. *J. geol. Soc. Lond.* **134**, 201–213.

England, P. & Thompson, A. B. 1984. Pressure–temperature–time paths of regional metamorphism 1. Heat transfer during the evolution of regions of thickened continental crust. *J. Petrol.* **25**, 894–928.

Gray, D. R. & Durney, D. W. 1979. Crenulation cleavage differentiation: implications of solution–deposition processes. *J. Struct. Geol.* **1**, 73–80.

Gray, N. H. & Busa, M. D. 1994. The three-dimensional geometry of simulated porphyroblast inclusion trails: inert-marker, viscous-flow models. *J. metamorph. Geol.* **12**, 575–587.

Hu, J. C. 1987. Regional metamorphism of medium pressure type as revealed by the Longmenshan metamorphic belt, Sichuan Province. In: *Contribution to Compilation and Study of Metamorphic Map of China* (1) (edited by Dong, S. B. & Shen, Q. H.). Geological Publishing House, Beijing, 126–137.

Hu, J. C. & You, Z. P. 1991. Metamorphic episodes in inner Longmenshan metamorphic belt. *Acta geol. Sichuan* **11**, 188–191.

Koons, P. O. 1987. Some thermal and mechanical consequences of rapid uplift: an example from the Southern Alps, New Zealand. *Earth Planet. Sci. Lett.* **86**, 307–319.

Koons, P. O. 1990. Two-sided orogen: collision and erosion from the sandbox to the Southern Alps, New Zealand. *Geology* **18**, 679–682.

Li, Y. T., Ying, D. G., Huang, Y. Z. & Hao, Z. W. 1975a. China Geological Map, scale 1:200 000, Maowen Sheet (H-48-II), Geological Press, Beijing.

Li, Y. T., Ying, D. G., Huang, Y. Z. & Hao, Z. W. 1975b. China Geological Survey Report, Maowen Sheet (H-48-II), Geological Press, Beijing.

Liu, Z. S., Wang, P. S., Fu, G. X. & Zhuang, Z. H. 1984. A preliminary study on the Changgou–Mengtonggou *S*-type granite in western Sichuan. *Contr. geol. Qinghai–Xizang (Tibet) Plateau* **15**, 209–219.

Long, X. M. 1991. Several questions of geochronic evolution in the mid-northern section of Longmen Shan mountains. *J. Chengdu Coll. Geol.* **18**, 8–16.

Meneilly, A. W. 1982. Regional structure and syntectonic granite intrusion in the Dalradian of the Gweebarra Bay area, Donegal. *J. geol. Soc. Lond.* **139**, 633–646.

Norris, R. J., Koons, P. O. & Cooper, A. F. 1990. The obliquely convergent plate boundary in the South Island of New Zealand: implications for ancient collision zones. *J. Struct. Geol.* **12**, 715–725.

Passchier, C. W., Trouw, R. A. J., Zwart, H. J. & Vissers, R. L. M. 1992. Porphyroblast rotation: *eppur si muove*? *J. metamorph. Geol.* **10**, 283–294.

Platt, J. P. & Vissers, R. L. M. 1980. Extensional structures in anisotropic rocks. *J. Struct. Geol.* **2**, 397–410.

Powell, D. & Treagus, J. E. 1969. On the geometry of *S*-shaped inclusion trails in garnet porphyroblasts. *Mineralog. Mag.* **36**, 453–456.

Powell, D. & Treagus, J. E. 1970. Rotational fabrics in metamorphic minerals. *Mineralog. Mag.* **37**, 800–814.

Powell, R. & Holland, T. J. B. 1988. An internally consistent thermodynamic data set with uncertainties and correlations: 3 Applications to geobarometry, worked examples and a computer program. *J. metamorph. Geol.* **6**, 173–204.

Powell, R. & Holland, T. J. B. 1990. Calculated mineral equilibria in the pelite system KFMASH (K_2O–FeO–MgO–Al_2O_3–SiO_2–H_2O). *Am. Miner.* **75**, 367–380.

Powell, R. & Holland, T. J. B. 1994. Optimal geothermometry and geobarometry. *Am. Miner.* **79**, 120–133.

Ramsay, J. G. & Graham, R. H. 1970. Strain variation in shear belts. *Can. J. Earth Sci.* **7**, 786–813.

Rosenfeld, J. L. 1970. Rotated garnets in metamorphic rocks. *Geol. Soc. Am. Spec. Pap.* **129**, 102 pp.

Tobisch, O. T. & Paterson, S. R. 1988. Analysis and interpretation of composite foliations in areas of progressive deformation. *J. Struct. Geol.* **10**, 745–754.

Visser, P. & Mancktelow, N. S. 1992. The rotation of garnet porphyroblasts around a single fold, Lukmanier Pass, Central Alps. *J. Struct. Geol.* **14**, 1193–1202.

Wilson, C. J. L., Chen, S., Worley, B. A., Arne, D., Luo, Z. & Liu, S. 1994. Tectonic evolution of the Longmen Mountains and Western Sichuan Foreland Basin. *Geol. Soc. Austr. Abstr.* **36**, 174–175.

Worley, B. A., Wilson, C. J. L., Liu, S. G. & Luo, Z. L. 1995. Structural observations from the Wenchuan–Maowen metamorphic Belt, Longmen Mountains, China. *J. Chengdu Inst. Tech.* **22**, 24–41.

Xu, G., Will, T. M. & Powell, R. 1994. A calculated petrogenetic grid for the system K_2O–FeO–MgO–Al_2O–SiO_2–H_2O, with particular reference to contact-metamorphosed pelites. *J. metamorph. Geol.* **12**, 99–119.

Yuan, H. H., Zhang, Z. L. & Zhang, P. 1991. The uplifting and cooling histories of the Laojungou granite in the western margin of the central section of the Longmen Mountains. *J. Chengdu Coll. Geol.* **18**, 17–22.

Zhang, Z. L., Zhang, P. & Yuan, H. H. 1991. The geochemical information of dynamical mechanism forming Longmenshan Mountains. *J. Chengdu Coll. Geol.* **18**, 23–32.